Consortium Members

Effects of Wildfires On Lakes

Study report: State of art and selection of study areas

Reference: CCI-LAKES-0076-CCN

Issue: 1.1

Date: 6 July 2022

Version history:			
Issue:	Date:	Reason for change:	Author
1.0	19 May 2022	Initial Version	G. Free et al.
1.1	06 July 2022	Revision following ESA review	G. Free

People involved in this issue:			Signature
Authors:		CNR	
	Daniela Stroppiana Gary Free Mariano Bresciani Monica Pinardi	CNR	
Approved by:	Bruno Coulon	CLS	Bruno Coulon Signature numérique de Bruno Coulon Date : 2022.07.13 02:38:42 +02'00'
Authorized by:	Clément Albergel	ESA	

Distribution:		
Company	**Names**	**Contact Details**
ESA	C. Albergel	Clement.Albergel@esa.int
CLS	B. Coulon B. Calmettes A. Mangilli P. Thibaut	bcoulon@groupcls.com bcalmettes@groupcls.com amangilli@groupcls.com pthibaut@groupcls.com
Eola	E. Zakharova	zavocado@gmail.com
H2OG	C. Duguay	claude.duguay@h2ogeomatics.com
LEGOS	J.F. Crétaux A. Kouraev	jean-francois.cretaux@legos.obs-mip.fr kouraev@legos.obs-mip.fr
PML	S. Simis	stsi@pml.ac.uk
CNR	C. Giardino	giardino.c@irea.cnr.it

List of Contents

1. Background

The research topic of the relationship between wildfires and water quality is largely inter-disciplinary involving.

Droughts and climate-change-driven warming lead to more frequent and intense wildfire. Wildfires can compromise water quality both during active burning and for months and years after the fire has been contained or extinguished. Burned watersheds are prone to increased flooding and erosion, which can negatively affect water-supply reservoirs, water quality, and drinking-water treatment processes. Fires have many direct and indirect effects on the environment including vegetation, wildlife, soil, air, and water. Several studies about burning impact on water quality and aquatic ecology have focused on intense wildfire events while few others reported about low to moderate intensity burning have been mixed with either minimal short-lived response, or substantial effects similar to wildfire if managed for a long enough period.

The impact of fires in changing water quality might be due to the atmospheric depositions of aerosols as well as from run off from the catchments. Whatever the reason, due to the complexity of interactions including vegetation, soil, topography, hydrology, climate, and atmosphere, effects of burning on water is likely to be highly site specific. Past studies mainly used two ways to examine effects of fire on water quality. Field sampling in accordance with the burn, and controlled lab extraction. However, field samples are hard to control, requires a lot of replications, and measurements are limited to the specific sites of measurement. Lab extraction experiments provide precise measurements and generates parameters such as hydrophobicity of the burned materials that are hard to obtain in the field, but are not as relatable to real conditions and can only cover a brief period. To fill such gaps remote sensing might provide useful information.

Major common concern about the relationship between fires and water quality is the impact of physical and chemical constituents on drinking water quality of major water reservoir (Smith et al., 2011). Various studies have investigated the relationship between fires and water quantity and quality, mainly focusing on their impacts on the quality of water supply in forest fire-prone watersheds (e.g., in U.S. and Australia) (Bladon et al., 2014; Oliver et al., 2012), while less fire-prone forest and non-forested watersheds were less analysed. Moreover, the effects of wildfires on water quality are less commonly reported compared to the effects on terrestrial ecosystems or on the hydrology of burned catchments (Dahm et al., 2015).

Forest land generally provides higher quality water supply compared to other land use; moreover, the presence of forested vegetation reduces flooding from storms that can increase suspended and dissolved constituents (Murphy et al., 2015). By contrast, forest catchments can be subject to wildfires that, in some regions of the world can be very intense and induce long lasting removal of the forest vegetation cover.

Various studies used remote sensing data to improve the understanding of effects of wildfires in aquatic ecosystems. In particular, the effect of aerosols deposition in oceans has been recently investigated by Tang et al. (2021) while Pacheco and Fernandes (2021) reviewed current research on the nexus wildfires-watershed hydrology-stream water quality. Tang et al. (2021) discussed about aerosol emissions from Australian wildfires leading to the atmospheric transport of macronutrients and bio-essential trace metals such as nitrogen and iron, respectively. Their work suggested that the oceanic deposition of wildfire aerosols can relieve nutrient limitations and, consequently, enhance marine productivity. Similarly, we might expect that similar processes might interest clear deep lakes. Actually Di Nicolantonio et al. (2015) used MERIS data for identifying the effect of Saharan dust deposition in an oligotrophic lake: the results reported on an increase of chlorophyll-a (chl-a) concentration as proxy of phytoplankton abundance was observed. With respect to effects of wildfires and in particular of runoff responding to burned areas the aquatic ecosystems can also respond. Given the complex interplay between the natural environment and spatiotemporal patterns of burned areas, the assessment of wildfire impacts on water quality of catchments might be challenging. Then as, the quality changes seem to last shorter than the hydrologic impacts the scientific literature into remote sensing studies has mostly addressed the hydrologic impacts looking into the consequences of sediment and ash discharge into the water masses, evapotranspiration, hydraulic regimes rather than to look at water quality changes, including turbidity nutrient, and metal contamination. Nevertheless, given wildfires impact water quality with potential sequels for aquatic biota (Rust et al., 2019a; Valenca et al., 2020; Oliveira et al., 2018), remote sensing-based investigation are still very relevant.

A study from Uzun et al. (2020) of three fires that occurred in the Northern California Coastal Ranges in 2015 evidenced high levels of turbidity (e.g., 871 ± 747 NTU for the Rocky fire), and total suspended solids (613 ± 626 mg/L) during the first rainy season postfire. According to (Rust et al., 2019b) wildfires commonly increase nutrient, carbon, sediment and metal inputs to streams, yet the factors responsible for the type, magnitude and duration of water quality effects are poorly understood. Prior work by the current authors found increased nitrogen, phosphorus and cation exports were common the first 5 post-fire years from a synthesis of 159 wildfires across the western United States.

2. Effect of wildfires on water quality

Two major pathways can be identified for the relationship between fires and water characteristics and conditions:

1. Transport of compounds from fire emissions and deposition over lake waters;
2. Increased soil erosion and changes in runoff due to vegetation removal and sediment transport through the river network to reservoir.

In both cases, rainfall plays a key role.

2.1. Atmospheric transport

Wildfires are a source of gas and aerosols including black carbon aerosols (BC) (Andreae et al., 1993; Chen et al., 2009). BC is recognized as a major pollutant originated from incomplete combustion of biomass and fossil fuel that, interacting with Earth's radiation balance and cloudiness affects regional and global climate as well as the environment and human health (Ramanathan and Carmichael, 2008).

Pollutants originated from wildfires through smoke plumes are transported into the atmosphere and, in some cases, far from the originating fire event location (Wang et al., 2022). Dry deposition is a key process responsible of the removal of aerosols from the atmosphere and water quality can be significantly affected although large uncertainty is still affecting the quantification of this process especially over remote regions (Popovicheva et al., 2021).

Popovicheva et al. (2021) analysed the spatio-temporal distribution of near water surface aerosols over lake Baikal, Russia, measured during ship expedition in 2018, and their correlation with significant fire events. Wildfires were found to affect aerosol composition over the lake surface especially in more remote regions of the northern Baikal Lake.

2.2. River network transport

Wildfires can have a significant geomorphological and hydrological impact on water catchments especially in relation to post-fire rainfall events that can trigger erosion, streamflow and transport processes leading to potential alteration of water quality of drinking reservoir (Shakesby and Doerr, 2006; Smith et al., 2011). The magnitude and duration of hydrological and geomorphological activity following wildfires depend on the complex interplay of factors including site (e.g. catchment size) and fire characteristics (e.g. burned area severity and extent) as well as post-fire rainfall patterns.

Changes in post-wildfire runoff and erosion are most severe during high-intensity rainfall (Moody et al 2013) especially when occurring close in time to the fire events when vegetation has little time to recover from fire. Indeed, the magnitude, intensity and frequency of post-fire rainfall and associated flow events are key drivers of erosion and sediment delivery in many burned catchments (Robichaud et al., 2007; Malmon et al., 2007; Cannon et al., 2008; Moody and Martin, 2009).

Changes induced by wildfires can last from a month to several years depending on the fire and site characteristics ('*window of disturbance*' as defined by Prosser and Williams, 1998).

Murphy et al. (2015) and literature cited showed increased turbidity, total suspended solids (TSS), dissolved organic carbon (DOC), and nitrate (NO_3) − concentrations downstream of a burned area in response to convective storms ten months to three years after wildfire in Colorado, US.

Smith et al. (2011) reviewed the effects of wildfires on the quality of water supply in forest catchments with focus on suspend sediments transport observing however that reporting of post-fire turbidity in streams and reservoirs is limited.

Smith et al. (2011) also observed that large storage reservoirs might reduce the magnitude and rate of change of TSS/turbidity inputs from tributary streams thus resulting in lower peak. Yet peaks in TSS/turbidity may last longer and could be better captured by continuous monitoring rather than ad-hoc event driven in situ measurements.

3. Remote sensing contribution

From the analysis of the literature, we observed that most of the literature relies on *in situ* sampling of water quality parameters (Smith et al., 2011) often on small plot and/or regions that are carried out in a wide range of conditions; in this framework generalization and comparability of the results and knowledge gained is very difficult.

Moreover, the quantification of the impact of wildfires on river and reservoir water quality is hampered by the unpredictable nature of fires and the distribution of monitoring network and/or the sampling regimes.

While detecting burned areas relies on the persistence of the burned signal, detecting changes in water constitutes concentration due to fires (or any other factor) depends on frequency of sampling and/or observations. Remote sensing can certainly improve frequency of observation and monitoring of water quality parameters compared to *in situ* measurements but there is still uncertainty on the likelihood of detecting changes. This uncertainty is a function of the variability of each constitute as well as of the hydrological characteristics of the lake and water catchment (Smith et al., 2011).

The impact of wildfires on water catchments can take advantages of systematic monitoring capabilities offered by remote sensing techniques; as pointed out by Smith et al. (2011), the impact of wildfires on TSS/turbidity depends on the size of the catchment and for larger reservoirs (e.g. Baikal, Russia) change in TSS/turbidity may be of lower intensity but longer duration thus observable only with systematic monitoring and/or sampling. RS can offer frequent data that can reduce monitoring effort and costs over large areas.

Despite the increased concern on the impact of wildfires on water quality of reservoir and the increased volume of literature works, an uneven coverage of the geographical distribution has been observed (Shakesby and Doerr, 2006). Moreover, the topic has mainly been addressed at small scales while there is a poor understanding at larger scales. The ESA CCI products could fill these gaps by providing global coverage of both fire regimes and water quality parameters also for the more remote regions of the world.

3.1. Remote sensing of fires

Remote sensing techniques can fill the gap of systematic monitoring of fires at regional to global scales for a comprehensive assessment of the impacts on water quality. Since fire occurrence is unpredictable, EO data can support systematic delivery of active fires and burned area products depicting the spatio-temporal distribution of fires and fire affected areas over all region of the world.

The use of satellite images for fire monitoring has a long history: since early 70s, a wide range of data sources and methods have been exploited (Chuvieco et al., 2019) with highly variable results in terms of product characteristics and accuracy.

Since the earliest attempts to map the presence of fires through the identification of an active fire (presence of the flaming fire front) and/or a burned area (extent of the area affected by fire) many works have been published. Several countries have recently developed fire monitoring systems relying on satellite data such as in the Monitoring Trends in Burn Severity (MTBS) (Eidenshink et al., 2007) and the Landsat Burned Area Essential Climate Variable (BAECV) (Hawbaker et al., 2017) in the United States and the European Forest Fire Information System (EFFIS) (San-Miguel-Ayanz et al., 2012).

These products are certainly an important reference at regional level implementing customized algorithm for harmonized fire products from medium resolution satellite data such as those provided by Landsat and Sentinel missions. However, to the aim of understanding the relationship between fires and water quality in lake reservoirs over a wide range of geographical regions and fire regimes, only operational products could be considered. The objectives of this project require consistent information on water quality parameters and fire occurrence to make results across geographic regions and study sites comparable. One of the first tasks will be the selection of suitable study sites that could be carried out in a robust way only if systematic monitoring of water quality and fires is available across countries.

To this aim, the project will rely on global BA products rather than regional fire products that might be hardly comparable from region to region. Indeed, global BA can provide a consistent picture of the areas affected by fires across regions of the World.

3.2. Global fire products

First attempts of global fire products were made in the late 90s early 2000s (Chuvieco et al., 2019). Object of these products have been both *active fires* (detection of the flaming front of the fire) and *burned areas* (detection of the vegetated surface affected by the fire) to depict spatio-temporal variability of vegetation fires. Active fire product delivers information on local to global scale fire activity a timely and accurate manner (Wooster et al., 2021) and rely on the identification of fire radiative strength (Fire Radiative Power; FRP) of fires that are actually consuming vegetation and/or organic soil at the time of satellite overpass. Active fire detection relies on the thermal signal to identify pixels containing actively burning fires. A burned area is the area affected by a fire that is characterized by the post-fire signal due to removal of vegetation and changes in vegetation structure and the deposit of combustion products (charcoal and ash) (Pereira et al.,1997).

Given the constraint that the fire has to be active at satellite overpass time to be detected and that only the thermal anomaly of the flaming front is detected, active fire mapping represents a spatio-temporal sampling of the extent of the area affected by vegetation fires. However, active fire detection provides more accurate temporal reporting of fire occurrence. On the contrary, the persistence of the burned area signal, being related to the damage occurred to vegetation, guarantees a more accurate and reliable assessment of the area affected by fires. Burned area mapping allows the detection of the surface affected by a fire after the event has exstinguished although the persistence of the signal is a function of several factors mong which fire characteristics and land cover characteristics and conditions.

At present four major fire products can be considered:

1. FireCCI51 (Burned Areas)
2. MCD64A1 c6 (Burned Areas)
3. NASA MCD14DL active fire product
4. NASA VIIRS active fire productNRT)

Table 1: Summary characteristics of the available global products for fire information.

Name	Source Data	Spatial resolution
FireCCI51	MODIS VIS/NIR	250 m / 0.25 deg
C6 MCD64A1	MODIS VIS/NOR/SWIR	500 m
MODIS active fires	MODIS TIR	1 km
VIIRS active fires	VIIRS TIR	375 m

3.2.1. FireCCI 51 BA product

The MODIS Fire_cci version 5.1 products (FireCCI51) (Lizundia-Loiola et al., 2020; Pettinari et al., 2021) comprise maps of global burned area covering the period 2001-2020 developed and tailored for use by climate, vegetation and atmospheric modellers, as well as by fire researchers or fire managers. The FireCCI51 product was first released on November 2018, with subsequent extensions to include BA for the years 2018 to 2020. It was obtained combining daily surface reflectance in the RED and near infrared (NIR) bands from MODIS at 250m resolution product (MOD09GQ Collection 6 images) and thermal information from the MODIS active fire products (MCD14ML Collection 6). Land cover information from the Land Cover CCI project (see section 2.8) has also been used. Details on the algorithm can be found in Lizundia-Loiola et al. (2020) and in Pettinari et al. (2021).

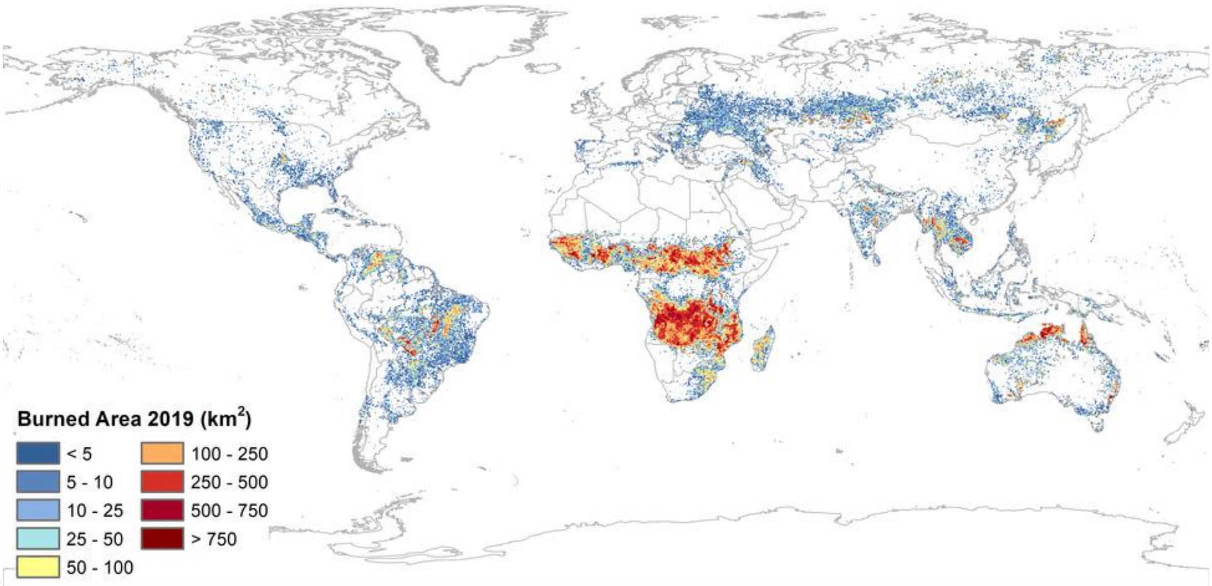

Figure 1: The FireCCI51 global BA map for the year 2019 (total burned area in km2) (source: https://geogra.uah.es/fire_cci/firecci51.php).

3.2.2. **MCD64A1 c6 BA product**

The latest version (Collection 6) of the MODIS Global Burned Area Product was released in 2017 (MCD64A1) and it replaced previous version to improve detection of small burned areas, to reduce burn-date temporal reporting accuracy and omission errors (https://modis-fire.umd.edu/).

The C6 MCD64A1 BA detection algorithm takes as input the MODIS daily surface reflectance (Vermote and Justice, 2002) (MOD09GHK and MYD09GHK) and the 1-km Terra (MOD14A1) and Aqua (MYD14A1) Level 3 daily active fire products (Justice et al., 2002) as well as MODIS MCD12Q1 annual land cover product. Full description of the C6 MCD64A1 BA product is available in Giglio et al. (2018) and in the MODIS Burned Area Product User's Guide (https://modis-fire.umd.edu/files/MODIS_C6_BA_User_Guide_1.3.pdf).

The BA algorithm identifies the date of burn for each 500 m grid cells within a MODIS tile and the MCD64A1 Burned Area Product is available as monthly BA maps, Level-3 gridded 500-m product containing per-pixel information on burning (burn date-DOY) and quality information at tile-level (e.g. date uncertainty, QA).

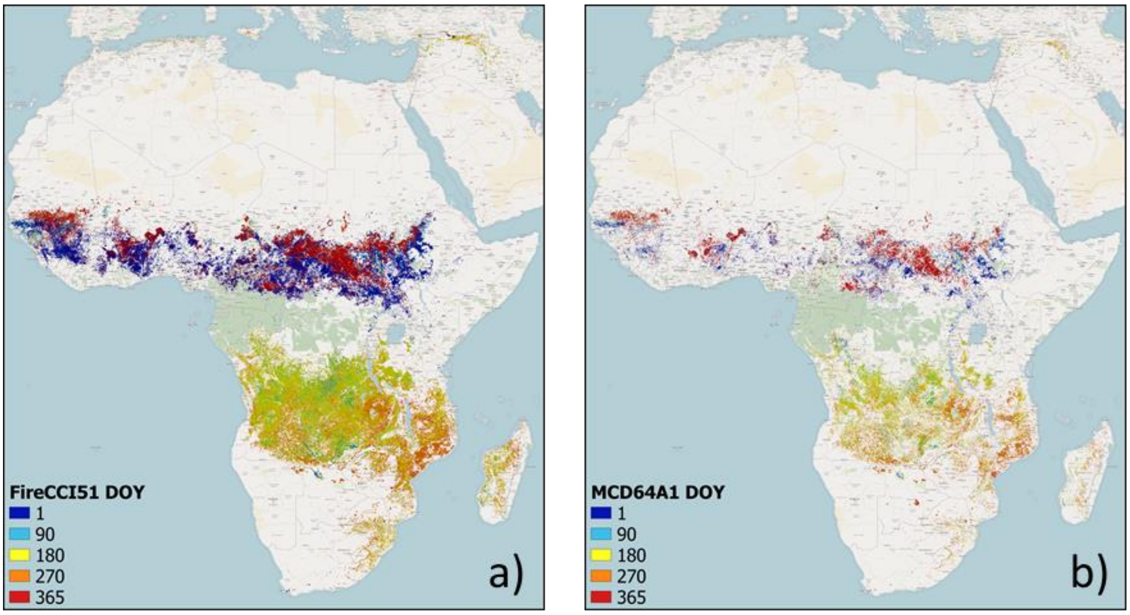

Figure 2: The Day Of Detection (DOY) of burned pixels for the FIRECCI51 (a) and the MODIS (b) BA products over continental Africa for the year 2019.

3.2.3. Active fire products

Currently there are two active fire products available to depict spatio-temporal distribution of fires over the globe derived from the NASA's Moderate Resolution Imaging Spectroradiometer (MODIS) aboard the Terra and Aqua satellites and NASA's Visible Infrared Imaging Radiometer Suite (VIIRS) aboard the joint NASA/NOAA Suomi National Polar orbiting Partnership (Suomi NPP) and NOAA-20 satellites. Active fire data can be downloaded from the NASA's Fire Information for Resource Management System (FIRMS) that distributes Near Real-Time (NRT) fire/thermal anomaly data within 3 hours of satellite observation as well as archive datasets (https://firms.modaps.eosdis.nasa.gov/map/#d:24hrs;@0.0,0.0,3z).

The MODIS active fire product delivers “fire pixels” that contain one or more actively burning fires at the time of the satellite overpass. The detection algorithm relies on 1-km MODIS channels brightness temperatures at 4-, 11-, and 12-μm wavelengths (Giglio et al., 2016) and it is applied to unprojected swath to classify each pixel as missing data, cloud, non-fire, fire, or unknown. The details of the algorithm and of the MOD14/MYD14 products are provided in the Product User's Guide (Giglio, 2015).

Combined (Terra and Aqua) MODIS active fire products (MCD14DL) are processed using the standard MOD14/MYD14 Fire and Thermal Anomalies algorithm and made available in FIRMS.

The second source of information for fire presence is available from the Visible Infrared Imaging Radiometer Suite (VIIRS) 375 m thermal anomalies / active fire product. Active fire information is derived from the VIIRS sensor aboard the joint NASA/NOAA Suomi National Polar-orbiting Partnership (Suomi NPP) and NOAA-20 satellites. The 375 m data complements the 1 km MODIS fire information with enhanced resolution and better detection of small fires. Details on the algorithm and product characteristics are available in the Product’s User Guide (https://viirsland.gsfc.nasa.gov/PDF/VIIRS_activefire_User_Guide.pdf).

4. Selection of lakes to focus on for lakes-fire cci CCN

The general approach to selecting sites will use the Source – Pathway – Receptor (SPR) approach to examining the 2024 lake dataset (CRDP 2.0.1, Carrea et al., 2022). This longstanding approach is currently employed in the EU under the Water Framework Directive as a conceptual model to aid the understanding of the potential impact of pollutants (Holdgate 1979; European Commission and Directorate-General for Environment, 2012). It focuses on identifying the sources of pollutants, their pathway to the receptors (the lakes) and their interrelationships, as these are likely key to the understanding of the manifestation of ecosystem alterations caused by wildfires in lakes. For example, the fire intensity, extent and vegetation type burnt are key to characterising the source, while the pathway if dominated by fluvial rather than atmospheric will be influenced by the timing, distribution and amount of precipitation. The degree of impact on the lake, the receptor, will depend on its specific characteristics such as redisence time and trophic state. For example, a wildfire may result in a nutrient load sufficient to dramatically alter the ecological charactersitcs of an oligotrophic lake but not for an already degraded eutrophic lake.

4.1. Wildfires

In this context the wildfires are the pollutant source and for the initial selection we have utilized the FireCCI51 product to estimate total burned area per year. This product has the benefit of having an estimate of the type of land cover burned, derived from the LC_cci v2.0.7 product (ESA 2017). This is important as the type and amount of biomass burnt has different implications for export of nutrients and organic matter to the lakes as well as potentially altering the hydrology of the catchment. We examined the distribution of vegetation types burned across the 2024 hydrologic areas for 2011 (using the Hydrobasins data (Lehner and Grill, 2013)), with the intention on focusing on alteration to tree land cover classes (bands 5-9 in FireCCI51 product). The year 2011 was selected as it was the year with highest burned area globally (Otón et al. 2021).

In order to identify and aggregate similar types of wildfires, in terms of land cover burned a hierarchical cluster analysis was carried out using Sørensen distance with flexible beta linkage (McCune and Mefford, 2016). The dendrogram was cut at 6 groups based on the minimization of the p value (Figure 3). Clusters 4,5 and 6 were characterized by wildfires, while cluster 1, the most abundant (1281 lakes), had few records of burned vegetation, as did clusters 2 and 3. Cluster 4 was characterized by burned evergreen coniferous forestry in Canada and North America (Table 2, Figure 4). Cluster 5 was dominated by crops or natural shrubbery being located in Eurasia with notable clusters in south America and Australia. Cluster 6 was more diverse but contained the most burned area of deciduous broad leaves, and was more common in the southern hemisphere especially Africa. Therefore, three key source types may be initially used to structure the analysis approach for site selection. Further reference in the final selection will be made to formal biome stratification (Figure 5).

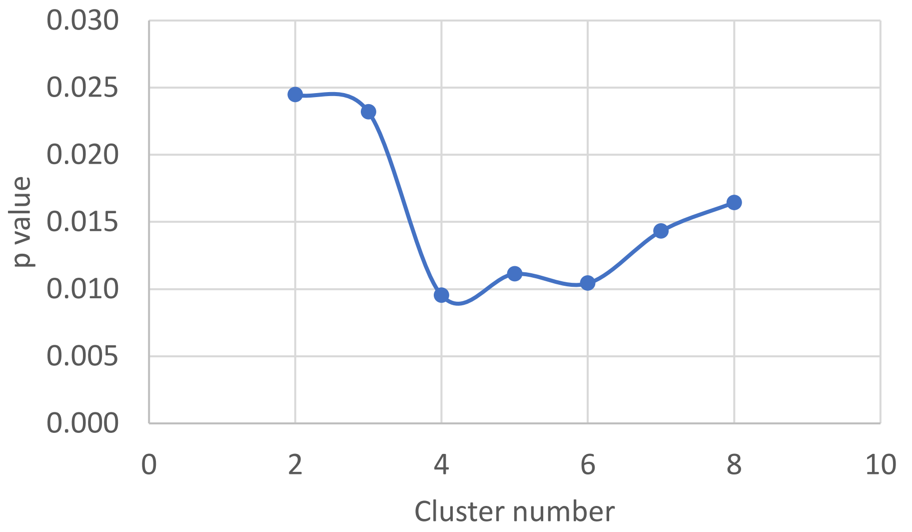

Figure 3: Average p for all land cover groups from an indicator species analysis of clusters 2 to 8. Minimum p (0.010) was reached after six clusters.

*Table 2: Indicator values for cluster analysis carried out on 2011 burned vegetation types (100% = perfect indicator i.e. LC burn occurs in only that cluster). *See appendix for full land cover details.*

	Cluster	1	2	3	4	5	6
	Cluster ID	1	883	1059	1348	1457	1648
	n	1281	145	152	95	180	171
LC code	**Land cover summary***						
LC01	Crop/Herb/shrub	0	0	2	0	**46**	**49**
LC02	Cropland	0	0	0	0	**21**	**23**
LC03	Crop/Natural	0	0	1	0	**22**	**71**
LC04	Crop/Natural	0	0	1	0	12	**81**
LC05	broadleaf, evergreen	0	0	0	0	1	**52**
LC06	broadleaf, deciduous	0	0	0	0	1	**84**
LC07	needleleaf, evergreen	0	2	0	**95**	1	0
LC08	needleleaf, deciduous	3	0	0	4	0	1
LC09	mixed leaf trees	0	0	1	**29**	3	5
LC10	tree/shrub	0	0	0	3	4	**81**
LC11	Herbs/trees/shrub	1	0	0	0	1	**60**
LC12	Shrubland	0	0	0	2	1	**81**
LC13	Grassland	0	0	0	0	6	**79**
LC14	Lichen/moss	0	0	0	**28**	0	0
LC15	Sparse veg	0	0	0	13	1	**22**
LC16	Trees flooded	0	0	0	**31**	0	12
LC17	Trees flooded	0	0	0	0	2	16
LC18	Shrubs/herbs flooded	0	0	0	0	4	**66**

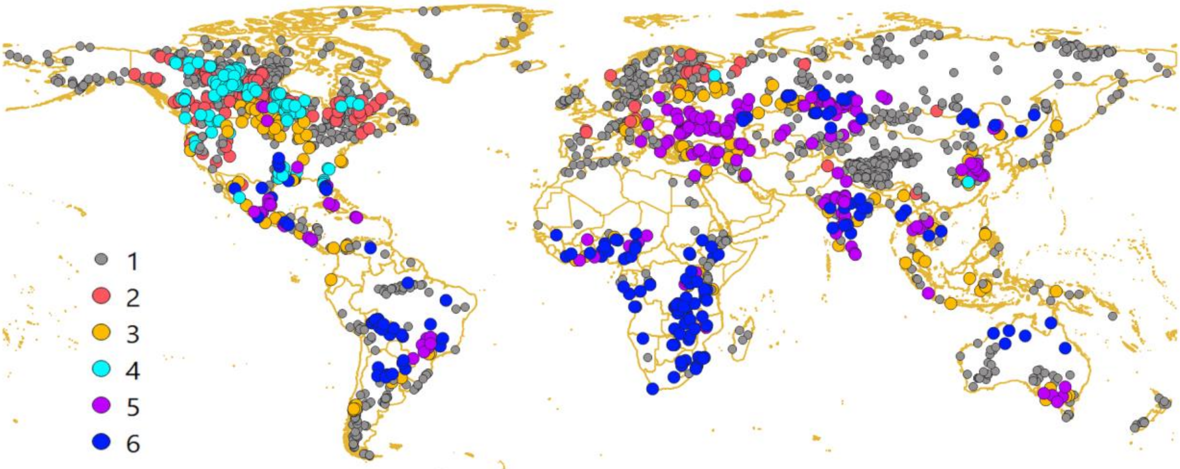

Figure 4: Map of six vegetation clusters burned in 2011. See Table 1 for LC indicator values of each cluster.

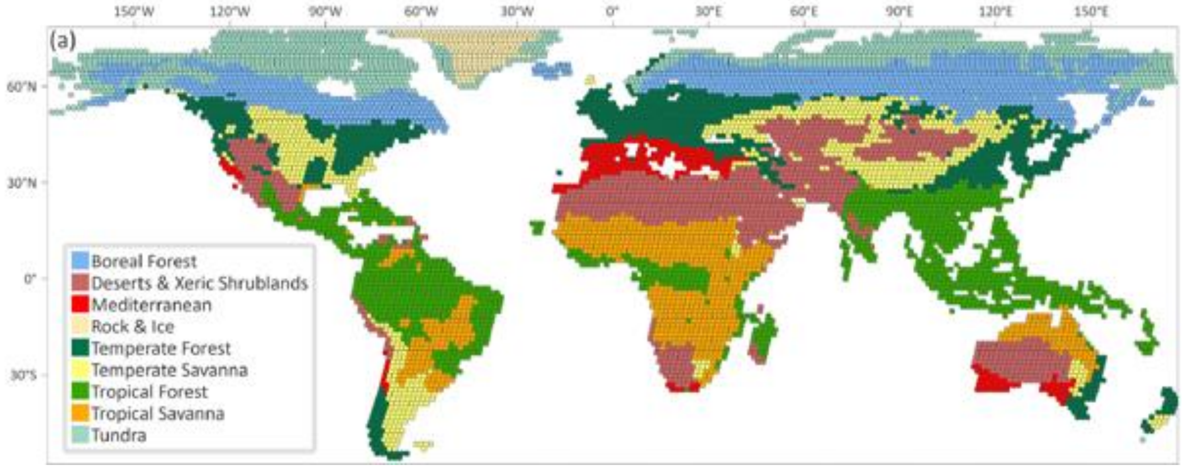

Figure 5: Biome stratification according to the 2017 map of the terrestrial ecoregions of the world. Taken from (Franquesa et al., 2022) based on data in (Dinerstein et al., 2017).

In addition, the proportion of the hydrological area estimated as burned area for the 20 years period (2001-2020) was also clustered. This should reveal groups with distinct amounts and patterns of burning. Six end groups were found (Figure 6). Cluster 10 was dominated by hydrological areas where a high proportion was burned every year, often in excess of 2-3% of the area. Similarly, cluster 6 burned every year but only 0.1-0.2% of the catchment area. The other groups had lower levels or no burnt area with the exception of clusters 80 and 35 that displayed peaks in the time series in the years 2013 and 2014 respectively. The spatial location of these clusters is shown in Figure 7 with notable similarities in distribution to Figure 4. Cluster 35 in 2014 clearly identifies the record wildfires in Canadian boreal forests that occurred that year (Walker et al., 2019). Joining the two approaches used we can derive a contingency matrix identifying lakes where the major wildfires occur for the different land cover types (Table 2). This should allow a selection of candidate lakes to cover geographical and land cover combinations with different burn temporal patterns (frequency/intensity) with a total of 314 lakes highlighted for further investigation.

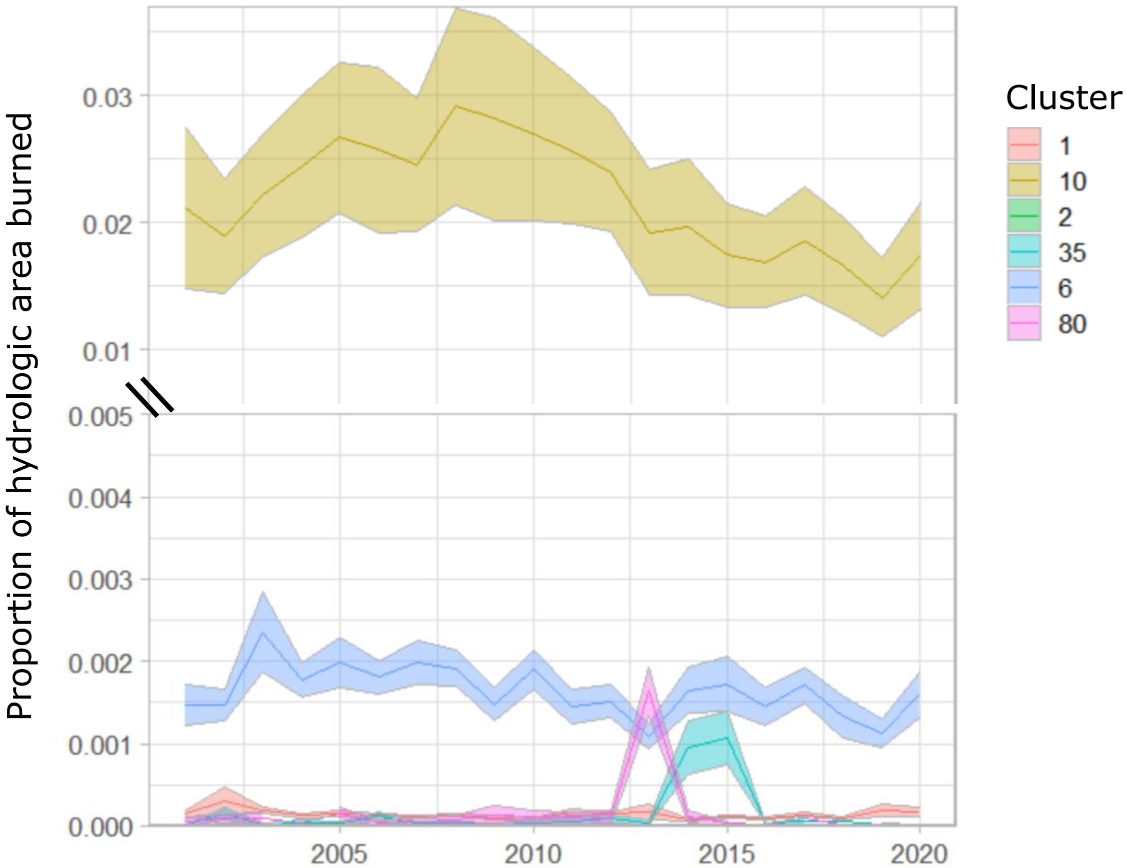

Figure 6: Proportion of hydrologic area burned by cluster number (2021-2020). Shaded area is 95% CI. Note scale break.

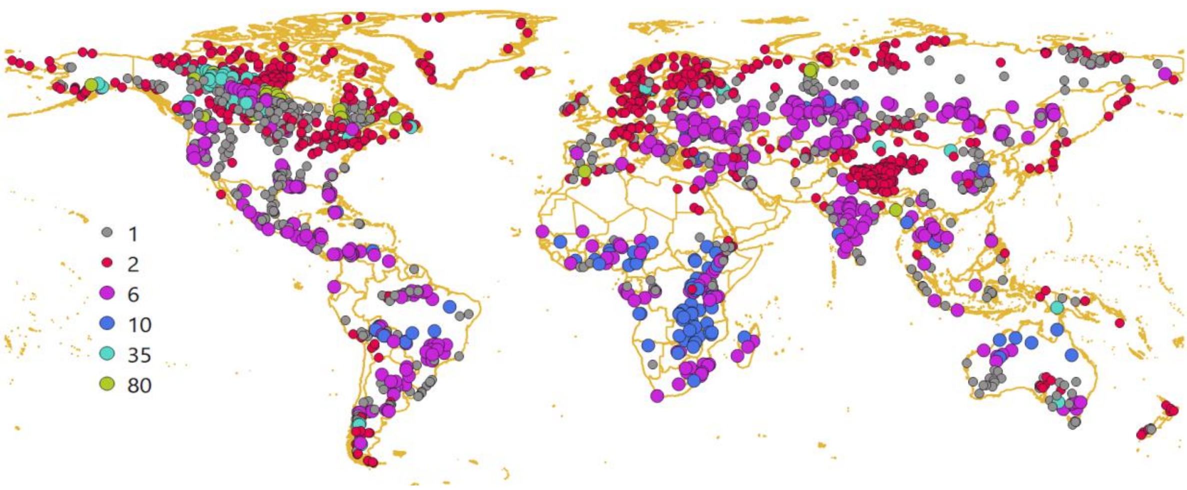

Figure 7: Map of six clusters derived from proportion of hydrologic area burned (2021-2020). See Figure 5 for area burned time series for each cluster.

Table 3: Contingency matrix of 2024 lakes selected via clustering of land cover burned (2011) and total area burned (2011-2020). Potential geographical and land cover combinations with burn temporal pattern (frequency/intensity) clusters are highlighted in bold (n = 314).

				Limited regular annual burning	**Significant regular annual burning**	**Limited peak noted in 2014**	**Limited peak noted in 2013**	
	Cluster	1	2	6	10	35	80	
								Total
	1	383	698	128	15	39	18	*1281*
	2	43	48	14	0	28	12	*145*
	3	71	19	53	6	1	2	*152*
Boreal forest (Canada)	4	54	10	**13**	0	**12**	**6**	*95*
Crops – natural shrubbery (Eurasia)	5	51	0	**114**	**13**	**1**	**1**	*180*
Deciduous broad leaves (Africa, India, South America)	6	17	0	**93**	**61**	0	0	*171*
	Total	*619*	*775*	*415*	*95*	*81*	*39*	*2024*

4.2. Pathway- transport to the lake

For examining the pathway of nutrients and organic material to the lake resulting from wildfires we will initially focus on terrestrial routes as these will allow also examination of alteration to the hydrologic pathways resulting from vegetation loss. Some of the most susceptible catchments may be those with a highly seasonal or variable rainfall that will result in overland flow. High rainfall events can sometimes account for large amounts of export, for example Kurz (2000) found that 41% of dissolved reactive phosphorous export for 16 months occurred between the 3rd and the 10th August 1997 when 150 mm of rain fell in four days in Ireland (Kurz, 2000).

We calculated the standardized precipitation index (SPI) for all of the lakes using ERA5 data with the reference period set to 1980-2010. Positive and negative SPI values indicate precipitation higher and lower than the median precipitation respectively (Vicente-Serrano et al. 2010; WMO, 2012; Beguería et al., 2017). This standardization has the benefit of allowing global comparisons. An example plot for lake Trasimeno, central Italy is shown in Figure 8. Values were calculated over a three- and twelve-month period, with the three-month estimation likely to be more useful in indicating precipitation above the norm in the short term that may actively transport material to the lake. The resulting SPI values can then be used to identify more dynamic systems, experiencing wildfires yet which can have high rainfall i.e. SPI values of 2.0+ (extremely wet) or 1.5 to 1.99 (very wet) (WMO, 2012). These can be used in the further selection of the 314 lakes. Opportunities can be taken to examine other pathways such as wet and dry deposition, potentially matching adjacent catchments and lakes without direct fire events in the catchment.

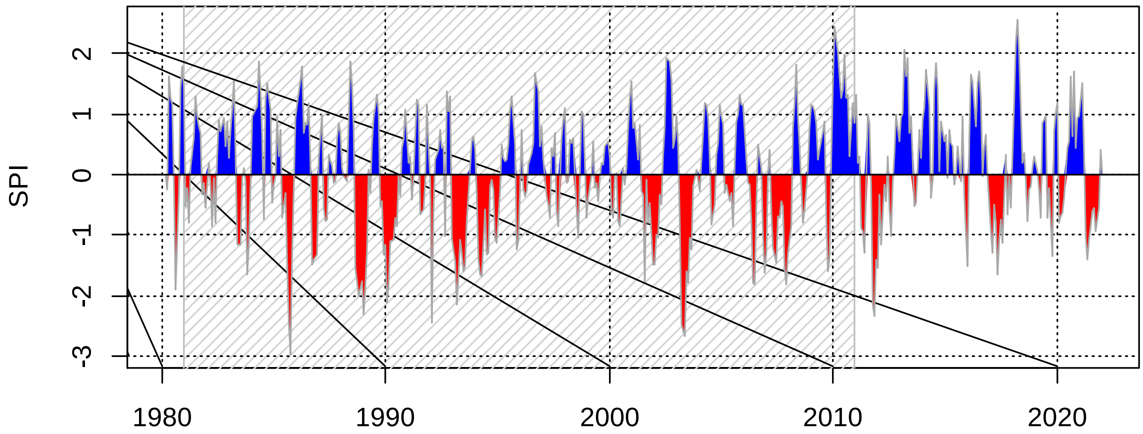

Figure 8: SPI values calculated over a three-month period for lake Trasimeno from 1980-2021. Shaded covers the 1981-2010 reference period.

4.3. **Lakes**

The lake is the receptor of material resulting from wildfires. One of the factors that moderates a lakes susceptibility to pollution from wildfires is its residence time. While an accurate estimation of the 2024 lakes is not possible, one useful descriptor is the catchment to lake area ratio which indicates the size of a lake relative to its catchment. A low value indicates that a lake is a substantial proportion of its catchment. It would be expected that such lakes would have long residence times and lake chemistry would be strongly influenced by internal processes. In addition, if the surface area of the lake is large enough, precipitation may make up a considerable proportion of lake volume, important for ash deposition (Schindler, 1971; Engstrom, 1987). In contrast, lakes with high catchment to lake area ratios would typically have short residence times and the effect of internal processes would be expected to be lower, except in summer when flushing is low. Therefore, water chemistry in these lakes will be more strongly influenced by their drainage area than internal processes compared to other lakes with a low catchment to lake area ratio. Catchment area data was obtained from the Hydrolakes database (Messager et al., 2016). The catchment area / lake area ratio was calculated for the lakes and plotted against the SPI for the 314 lakes selected from the fire products (see contingency matrix in Table 3) (Figure 9). This should allow us to identify those lakes that are likely to be more susceptible to wildfires in their catchments. Specifically, lakes with a 95th percentile SPI above 1.5 and a catchment to lake ratio above 30 (upper right in Figure 9). The list of 154 lakes thus selected is presented in Appendix 2. The next step is to use the lakes_cci products (chlorophyll-a and turbidity) to carry out a review of these lakes for data completeness and to base the selection on key biomes and fire regimes – as represented by the four clusters in Figure 9. A key consideration will be to include oligotrophic lakes in the selection as an impact from wildfires may not be visible in eutrophic lakes that are typically more variable and subject to catchment pollution sources.

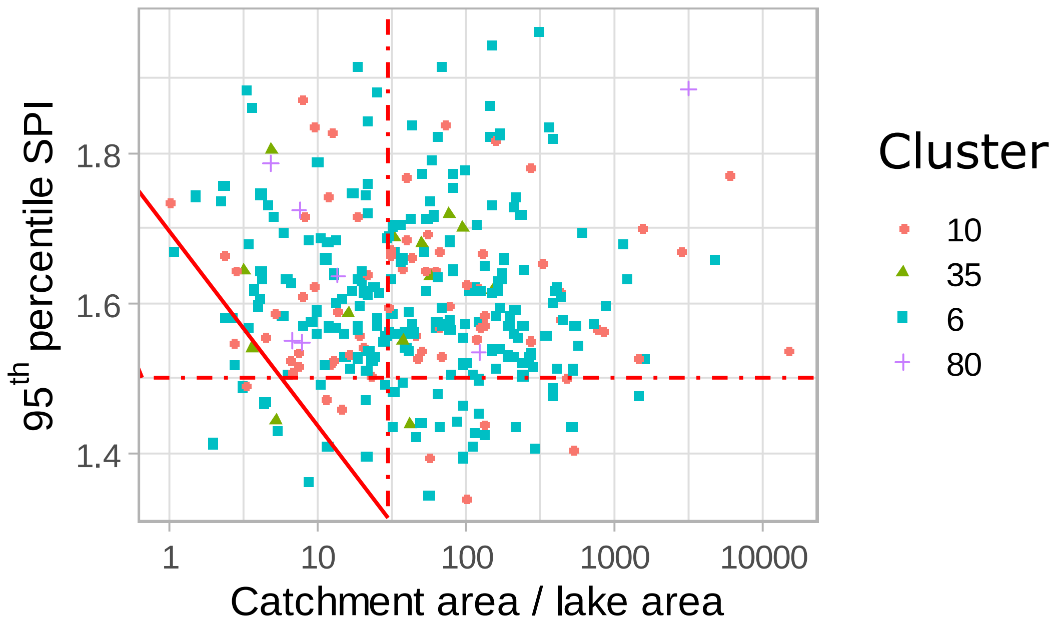

Figure 9: Lakes from contingency table 2 further selected to have a SPI 95th percentile above 1.5 and a catchment area / lake area above 30 (i.e. upper right quarter of graph).

5. References

Andreae, M.O., 1993. The influence of tropical biomass burning on climate and the atmospheric environment. Biogeochem Global Change, pp. 113–150.

Beguería, S., Vicente-Serrano, S.M., Beguería M.S., 2017. Package ‘spei.’ Calculation of the Standardised Precipitation-Evapotranspiration Index.

Belenguer-Plomer, M.A., Pettinari, M.L., 2016. ESA Climate Change Initiative–Fire_cci D3. 3.5 Product User Guide–Sentinel-1 South America. 2.1. 2.1 ESA.

Bladon, K. D., Emelko, M. B., Silins, U., Stone, M., 2014. Wildfire and the future of water supply, Environmental Science & Technology 2014 48 (16), 8936-8943.

Carrea, L., Crétaux, J.-F., Liu, X., Wu, Y., et al., 2022. ESA Lakes Climate Change Initiative (Lakes_cci): Lake products, Version 2.0.1. NERC EDS Centre for Environmental Data Analysis, date of citation. https://catalogue.ceda.ac.uk/uuid/03c935c6890c4b2ebf4aae4d84cd9472

Chen, Y., Zhi, G., Feng, Y., Liu, D., Zhang, G., Li, J., Sheng, G., Fu, J., 2009. Measurements of black and organic carbon emission factors for household coal combustion in China: implication for emission reduction. Environ. Sci. Tech. 43, 9495–9500.

Chuvieco, E., Mouillot, F., van der Werf, G.R., et al., 2019. Historical background and current developments for mapping burned area from satellite earth observation. Remote Sens. Environ. 225, 45–64.

Di Nicolantonio, W., Cazzaniga, I., Cacciari, A., Bresciani, M., Giardino, C., 2015. Synergy of multispectral and multisensors satellite observations to evaluate desert aerosol transport and impact of dust deposition on inland waters: study case of Lake Garda. Journal of Applied Remote Sensing, 9(1), 095980.

Dinerstein, E., Olson, D., Joshi, A., et al., 2017. An Ecoregion-Based Approach to Protecting Half the Terrestrial Realm. BioScience 67: 534–545.

Eidenshink, J., Schwind, B., Brewer, K., Zhu, Z.-L., Quayle, B., Howard, S., 2007. A project for monitoring trends in burn severity. Fire Ecol. 3, 3–21.

Engstrom, D.R., 1987. Influence of Vegetation and Hydrology on the Humus Budgets of Labrador Lakes. Can. J. Fish. Aquat. Sci. 44: 1306–1314.

ESA., 2017. Land Cover CCI Product User Guide Version 2. Tech. Rep. Available at:

http://maps.elie.ucl.ac.be/CCI/viewer/download/ESACCI-LC-Ph2-PUGv2_2.0.pdf.

European Commission and Directorate-General for Environment. 2012. Guidance on preventing or limiting direct and indirect inputs in the context of the groundwater directive 2006/118/EC. Guidance document No 17, Publications Office.

Franquesa, M., Lizundia-Loiola, J., Stehman, S.V., Chuvieco E., 2022. Using long temporal reference units to assess the spatial accuracy of global satellite-derived burned area products. Remote Sensing of Environment 269: 112823.

Giglio, L., 2015. MODIS collection 6 active fire product user's guide, revision A Technical Report, University of Maryland, (URL: http://modisfire.umd.edu/files/MODIS_C6_Fire_User_Guide_A.pdf).

Giglio, L., Boschetti, L., Roy, D.P., Humber, M.L., Justice, C.O., 2018. The Collection 6 MODIS burned area mapping algorithm and product. Remote Sens. Environ. 217, 72–85.

Giglio, L., Schroeder, W., Justice, C.O., 2016. The collection 6 MODIS active fire detection algorithm and fire products, Remote Sensing of Environment, 178, 31-41.

Hawbaker, T.J., Vanderhoof, M.K., Beal, Y.-J., Takacs, J.D., Schmidt, G.L., Falgout, J.T., Williams, B., Fairaux, N.M., Caldwell, M.K., Picotte, J.J., 2017. Mapping burned areas using dense time-series of Landsat data. Remote Sens. Environ. 198, 504–522.

Holdgate, M.W., 1979. A perspective of environmental pollution, Cambridge University Press.

Justice C.O., Giglio L., Korontzi S., Owens J., Morisette J.T., Roy D., Descloitres J., Alleaume S., Petitcolin F., Kaufman Y., 2002. The MODIS fire products Remote Sens. Environ., 83, pp. 244-262.

Kurz, I., 2000. Phosphorus exports from agricultural grassland with overland flow and drainage water (Johnstown Castle), p. 9–56. In Quantification of phosphorus loss from soil to water, final report and literature review. EPA.

Lehner, B., Grill. G., 2013. Global river hydrography and network routing: baseline data and new approaches to study the world’s large river systems. Hydrological Processes 27: 2171–2186. doi:10.1002/hyp.9740

Lizundia-Loiola, J., Pettinari, M. L., Chuvieco, E., Storm, T., Gómez-Dans, J. 2018. ESA CCI ECV Fire Disturbance: Algorithm Theoretical Basis Document-MODIS, version 2.0. Fire_cci_D2.1.3_ATBD-MODIS_v2.0. Available at https://esa-fire-cci.org/documents.

McCune, B., Mefford, M.J., 2016. PC-ORD. Multivariate Analysis of Ecological Data., MjM Software.

Messager, M.L., Lehner, B., Grill, G., Nedeva, I., Schmitt, O., 2016. Estimating the volume and age of water stored in global lakes using a geo-statistical approach. Nat Commun 7: 13603. doi:10.1038/ncomms13603

Murphy, S.F., Writer, J.H., Blaine McCleskey, R., Martin, D.A., 2015. The role of precipitation type, intensity, and spatial distribution in source water quality after wildfire, Environmental Research Letters, 10(8), DOI 10.1088/1748-9326/10/8/084007.

Oliveira-Filho, E.C., Brito, D.Q., Dias, Z.M., Guarieiro, M.S., Carvalho, E.L., Fascineli, M.L., Niva, C.C. Grisolia, C.K., 2018. Effects of ashes from a Brazilian savanna wildfire on water, soil and biota: An ecotoxicological approach. Science of the Total Environment, 618, pp.101-111.

Oliver, A.A., Reuter, J.E., Heyvaert, A.C. et al., 2012. Water quality response to the Angora Fire, Lake Tahoe, California. Biogeochemistry 111, 361–376.

Otón, G., Pereira, J.M.C., Silva, J.M.N., Chuvieco, E., 2021. Analysis of Trends in the FireCCI Global Long Term Burned Area Product (1982–2018). Fire 4: 74.

Pacheco, F.A., Fernandes, L.F.S., 2021. Hydrology and stream water quality of fire-prone watersheds. Current Opinion in Environmental Science & Health, 21, 100243.

Pereira, J.M.C., Sa, A.C.L., Sousa, A.M.O., Silva, J.M.N., Santos, T.N., Carreiras, J.M.B., 1999. Spectral characterisation and discrimination of burnt areas. In: Chuvieco, E. (Ed.), Remote Sensing of Large Wildfires in the European Mediterranean Basin. Springer-Verlag, Berlin, pp. 123–138.

Pettinari, M.L., Lizundia-Loiola, J., Chuvieco E., 2021. ESA CCI ECV Fire Disturbance: D4.2.1 Product User Guide - MODIS, version 1.1. Available at: https://climate.esa.int/en/projects/fire/key-documents/

Popovicheva, O., Molozhnikova, E., Nasonov, S., Potemkin, V., Penner, I., Klemasheva, M., Marinaite, I., Golobokova, L., Vratolis, S., Eleftheriadis, K., Khodzher, T., 2021. Industrial and wildfire aerosol pollution over world heritage Lake Baikal. Journal of Environmental Sciences, 107, 49-64.

Prosser, I.P., Williams, L., 1998. The effect of wildfire on runoff and erosion in native Eucalyptus forest, Hydrological Processes, 12 (2), 251 – 265.

Ramanathan, V., Carmichael, G., 2008. Global and regional climate changes due to black carbon. Nature Geosci 1, 221–227.

Rust, A.J., Randell, J., Todd, A.S., Hogue, T.S., 2019a. Wildfire impacts on water quality, macroinvertebrate, and trout populations in the Upper Rio Grande Ecol Manag, 453, p. 117636

Rust, A.J., Saxe, S., McCray, J., Rhoades, C.C. and Hogue, T.S., 2019b. Evaluating the factors responsible for post-fire water quality response in forests of the western USA. International Journal of Wildland Fire, 28(10), pp.769-784.

San-Miguel-Ayanz, J., Schulte, E., Schmuck, G., Camia, A., Strobl, P., Liberta, G., Giovando, C., Boca, R., Sedano, F., Kempeneers, P., 2012. Comprehensive monitoring of wildfires in Europe: the European forest fire information system (EFFIS). Approaches to Managing Disaster-Assessing Hazards. Emergencies and Disaster Impacts 87–108 (Rijeka: InTech.).

Schindler, D.W. 1971. A Hypothesis to Explain Differences and Similarities Among Lakes in the Experimental Lakes Area, Northwestern Ontario. J. Fish. Res. Bd. Can. 28: 295–301.

Scholten, R.C., Jandt, R., Miller, E.A., Rogers, B.M., Veraverbeke S., 2021. Overwintering fires in boreal forests. Nature 593: 399–404.

Shakesby, R.A., Doerr, S.H., 2006. Wildfire as a hydrological and geomorphological agent, Earth-Science Reviews, 74 (3-4), 269-307.

Smith H.G., G.J. Sheridan, P.N.J. Lane, P. Nymana, S. Haydon, 2011. Wildfire effects on water quality in forest catchments: A review with implications for water supply, Journal of Hydrology 396, pp. 170–192.

Tang, W., Llort, J., Weis, J., Perron, M. M., Basart, S., Li, Z., et al., 2021. Widespread phytoplankton blooms triggered by 2019–2020 Australian wildfires. Nature, 597(7876), 370-375.

Uzun, H., Dahlgren, R.A., Olivares, C., Erdem, C.U., Karanfil, T., Chow, A.T., 2020. Two years of post-wildfire impacts on dissolved organic matter, nitrogen, and precursors of disinfection by-products in California stream waters. Water Research, 181, p.115891.

Valenca, R., Ramnath, K., Dittrich, T.M., Taylor, R.E., Mohanty, S.K., 2020. Microbial quality of surface water and subsurface soil after wildfire. Water Research, 175, p.115672.

Vermote E.F., Justice N.Z.E.S.C.O., 2002. Operational atmospheric correction of the MODIS data in the visible to middle infrared: first results Remote Sens. Environ., 83, pp. 97-111.

Vicente-Serrano, S.M., Beguería, S., López-Moreno J.I., 2010. A Multiscalar Drought Index Sensitive to Global Warming: The Standardized Precipitation Evapotranspiration Index. Journal of Climate 23: 1696–1718.

Walker, X.J., Baltzer, J.L., Cumming, S.G., et al., 2019. Increasing wildfires threaten historic carbon sink of boreal forest soils. Nature 572: 520–523.

Wang, Y., Chen, H.-H., Tang, R., He, D., Lee, Z., Xue, H., Wells, M., Boss, E., Chai, F., 2022. Australian fire nourishes ocean phytoplankton bloom, Science of The Total Environment, 807, Part 1, 150775, ISSN 0048-9697.

WMO. 2012. Standardized precipitation index user guide, World Metrological Organisation.

Wooster, M.J., Roberts, G.J., Giglio, L., Roy, D.P., et al., 2021. Satellite remote sensing of active fires: History and current status, applications and future requirements, Remote Sensing of Environment, 267, 112694.

6. Annex

Table A1: Land cover categories (extracted from LC_cci). Source Fire_cci, Product User Guide (Belenguer-Plomer and Pettinari, 2016).

LC number	Class name	Fire_cci number
0	No data	**0**
10	Cropland, rainfed	**10**
11	*Herbaceous cover*	***10***
12	*Tree or shrub cover*	***10***
20	Cropland, irrigated or post-flooding	**20**
30	Mosaic cropland (>50%) / natural vegetation (tree, shrub, herbaceous cover) (<50%)	**30**
40	Mosaic natural vegetation (tree, shrub, herbaceous cover) (>50%) / cropland (<50%)	**40**
50	Tree cover, broadleaved, evergreen, closed to open (>15%)	**50**
60	Tree cover, broadleaved, deciduous, closed to open (>15%)	**60**
61	*Tree cover, broadleaved, deciduous, closed (>40%)*	**60**
62	*Tree cover, broadleaved, deciduous, open (15-40%)*	**60**
70	Tree cover, needleleaved, evergreen, closed to open (>15%)	**70**
71	*Tree cover, needleleaved, evergreen, closed (>40%)*	***70***
72	*Tree cover, needleleaved, evergreen, open (15-40%)*	***70***
80	Tree cover, needleleaved, deciduous, closed to open (>15%)	**80**
81	*Tree cover, needleleaved, deciduous, closed (>40%)*	***80***
82	*Tree cover, needleleaved, deciduous, open (15-40%)*	***80***
90	Tree cover, mixed leaf type (broadleaved and needleleaved)	**90**
100	Mosaic tree and shrub (>50%) / herbaceous cover (<50%)	**100**
110	Mosaic herbaceous cover (>50%) / tree and shrub (<50%)	**110**
120	Shrubland	**120**
121	*Shrubland evergreen*	***120***
122	*Shrubland deciduous*	***120***
130	Grassland	**130**
140	Lichens and mosses	**140**
150	Sparse vegetation (tree, shrub, herbaceous cover) (<15%)	**150**
152	*Sparse shrub (<15%)*	***150***
153	*Sparse herbaceous cover (<15%)*	***150***
160	Tree cover, flooded, fresh or brackish water	**160**
170	Tree cover, flooded, saline water	**170**
180	Shrub or herbaceous cover, flooded, fresh/saline/brackish water	**180**

Note: Only the level 1 classes are considered, so the subdivisions have the number of broader categories. Only vegetated LC classes have been considered.

Table A2: short list of selected lakes.

id	Name	Countries	Continent	lat	lon	Lake area (km2)	Catch area / lake area	95ile SPI	Cluster 20yr
GLWD00000337	Stephens	Canada	NA	56.42	-95.09	317	3129	1.89	80
HYLA00003271	None	Canada	NA	64.82	-116.48	35	121	1.53	80
GLWD00000226	Aylmer	Canada	NA	64.15	-108.45	801	50	1.68	35
GLWD00000275	Clinton-Colden	Canada	NA	63.94	-107.44	595	76	1.72	35
GLWD00000334	Artillery	Canada	NA	63.18	-107.79	516	94	1.70	35
GLWD00001058	Mamawi	Canada	NA	58.62	-111.46	146	151	1.62	35
GLWD00000746	Lake Maurepas	United States	NA	30.26	-90.50	237	33	1.69	35
GLWD00001422	Hindmarsh	Australia	OC	-36.04	141.91	129	57	1.64	35
GLWD00000011	Great Slave	Canada	NA	62.00	-112.39	26734	37	1.55	35
GLWD00000116	Kainji	Nigeria	AF	10.56	4.55	1035	1518	1.70	10
GLWD00000030	Albert	The Democratic Republic of the Congo;Uganda	AF	1.88	31.14	5527	75	1.60	10
GLBL00000013	Kyoga	Uganda	AF	1.58	32.46	2788	114	1.55	10
GLWD00000036	Mweru	The Democratic Republic of the Congo;Zambia	AF	-9.02	28.70	5043	43	1.66	10
GLWD00000510	Grajau	Brazil	SA	-6.92	-44.18	311	274	1.55	10
GLWD00000851	Tenis	Russian Federation	EU	56.13	71.94	252	46	1.56	10
HYLA00001509	None	India	AS	18.95	78.29	336	269	1.78	10
GLWD00000386	Manantali	Mali	AF	13.07	-10.37	438	64	1.57	10
GLWD00000274	Roseires Reservoir	Sudan	AF	11.55	34.46	225	839	1.56	10
HYLA00001551	Maga	Cameroon	AF	10.80	14.96	116	30	1.67	10
GLWD00000108	Kossour Reservoir	CÃ´te d'Ivoire	AF	7.32	-5.71	500	66	1.67	10
HYLA00001612	None	United Republic of Tanzania	AF	-7.02	35.84	444	157	1.82	10
GLWD00001046	Kabamba	The Democratic Republic of the Congo	AF	-7.89	27.04	109	1442	1.53	10
GLWD00000674	Kisale	The Democratic Republic of the Congo	AF	-8.27	26.51	298	425	1.62	10
GLWD00000314	Upemba	The Democratic Republic of the Congo	AF	-8.62	26.39	608	118	1.62	10
HYLA00001619	None	Angola	AF	-8.96	14.03	123	61	1.64	10
GLWD00001943	Chiuta	Malawi;Mozambique	AF	-14.62	35.88	144	30	1.67	10
GLWD00000586	Malombe	Malawi	AF	-14.68	35.25	310	422	1.58	10
GLWD00000462	Itezhi-Tezhi-Dam	Zambia	AF	-15.69	25.98	329	326	1.65	10
GLWD00000098	Argyle	Australia	OC	-16.36	128.67	829	55	1.69	10
HYLA00015836	None	Nigeria	AF	9.78	12.02	69	761	1.57	10
HYLA00015875	None	Sudan	AF	7.43	30.58	35	14510	1.54	10
HYLA00015901	None	Togo	AF	6.25	1.41	50	132	1.57	10

id	Name	Countries	Continent	lat	lon	Lake area (km2)	Catch area / lake area	95ile SPI	Cluster 20yr
HYLA00016017	None	United Republic of Tanzania	AF	-3.87	35.89	50	125	1.67	10
HYLA00016110	None	Zambia	AF	-8.91	29.78	38	39	1.77	10
HYLA00016120	None	The Democratic Republic of the Congo	AF	-10.03	27.25	42	37	1.65	10
HYLA00016145	None	Zambia	AF	-14.11	29.09	59	129	1.58	10
HYLA00016205	None	Australia	OC	-17.06	123.96	41	39	1.69	10
HYLA00016223	Manyame	Zimbabwe	AF	-17.80	30.53	75	53	1.64	10
HYLA00016225	Chivero	Zimbabwe	AF	-17.90	30.79	23	99	1.62	10
HYLA00016238	None	Zimbabwe	AF	-19.03	30.26	22	123	1.57	10
GLWD00000024	Volta	Ghana	AF	7.48	0.10	6045	67	1.53	10
GLWD00000306	Lagdo	Cameroon	AF	8.88	13.95	623	50	1.54	10
GLWD00000613	Tshangalele	The Democratic Republic of the Congo	AF	-10.92	27.05	180	70	1.84	10
GLWD00000506	Jebba	Nigeria	AF	9.44	4.61	275	5862	1.77	10
CGL200000012	Etosha-Pan	Namibia	AF	-18.76	16.34	40	2787	1.67	10
HYLA00015969	None	Uganda	AF	-1.22	29.67	21	46	1.53	10
GLWD00000014	Chad	Chad;Niger;Nigeria	AF	13.48	14.13	18752	52	1.67	6
GLWD00000023	Athabasca	Canada	NA	59.11	-109.88	7529	39	1.54	6
GLWD00000153	Chapala	Mexico	NA	20.24	-103.10	1052	42	1.71	6
GLWD00000129	Repressa de Jupia	Brazil	SA	-19.80	-50.51	1077	346	1.56	6
GLWD00000093	Krasnoyarskoye	Russian Federation	EU	54.85	90.96	1630	179	1.66	6
GLWD00000190	Novosibirskoye	Russian Federation	EU	54.30	81.78	1024	223	1.55	6
GLWD00000033	Kuybyshevskoye	Russian Federation	EU	54.61	48.67	5060	238	1.50	6
GLWD00000113	Saratov Reservoir	Russian Federation	EU	52.49	48.16	1073	1201	1.63	6
GLWD00000040	Zaysan	Kazakhstan	AS	48.72	83.43	4194	34	1.56	6
GLWD00000075	Hulun	China	AS	48.95	117.40	2121	63	1.57	6
GLWD00000079	Kakhovskoye	Ukraine	EU	47.26	33.95	2092	233	1.50	6
GLWD00000109	Hungtze	China	AS	33.33	118.73	1374	120	1.57	6
GLWD00000156	Eyasi	United Republic of Tanzania	AF	-3.59	35.12	1200	51	1.77	6
CGL200000008	Sua-Pan	Botswana	AF	-20.57	26.06	2962	217	1.74	6
GLWD00001640	Davy	Canada	NA	58.87	-108.29	111	78	1.56	6
GLWD00000546	Pend-Oreille	United States	NA	48.13	-116.38	360	174	1.63	6
GLWD00001344	Oologah	United States	NA	36.55	-95.61	115	97	1.57	6
GLWD00001368	Kissimmee	United States	NA	27.90	-81.27	121	33	1.67	6
GLWD00000266	Inhernillo	Mexico	NA	18.55	-101.87	288	381	1.82	6
GLWD00000477	Malpaso	Mexico	NA	17.12	-93.49	292	118	1.70	6
GLWD00001007	Guarico	Bolivarian Republic of Venezuela	SA	9.04	-67.39	188	43	1.57	6
GLWD00000238	das Brisas	Brazil	SA	-18.31	-48.94	333	285	1.51	6
GLWD00000494	Agua-Vermelha	Brazil	SA	-19.95	-49.88	507	275	1.53	6

id	Name	Countries	Continent	lat	lon	Lake area (km2)	Catch area / lake area	95ile SPI	Cluster 20yr
GLWD00000553	Jupia	Brazil	SA	-20.58	-51.52	289	1563	1.53	6
HYLA00000946	Promissao	Brazil	SA	-21.46	-49.50	511	110	1.51	6
GLWD00000199	Iepe	Brazil	SA	-22.83	-50.99	407	208	1.53	6
GLWD00000960	Malyye Chany	Russian Federation	EU	54.57	77.96	204	104	1.62	6
GLWD00000436	Kyivs'Ke-Reservoir	Ukraine	EU	50.92	30.50	636	386	1.60	6
GLWD00000229	Barun-Torey	Mongolia;Russian Federation	AS;EU	50.07	115.81	804	31	1.58	6
GLWD00000502	Bolon'	Russian Federation	EU	49.84	136.37	324	40	1.54	6
GLWD00001286	Karasor	Kazakhstan	AS	49.87	75.56	147	54	1.62	6
GLWD00000291	Buir	China;Mongolia	AS	47.81	117.70	598	36	1.70	6
GLWD00001609	Uyaly	Kazakhstan	AS	46.43	81.28	123	167	1.59	6
GLWD00000601	Krasnodarskoye	Russian Federation	EU	44.99	39.26	269	167	1.54	6
GLWD00000296	Chardarinskoye	Kazakhstan;Uzbekistan	AS	41.14	68.12	745	268	1.53	6
GLWD00000328	Mingechaurskoye	Azerbaijan	AS	40.92	46.75	416	148	1.54	6
GLWD00000542	Karakaya	Turkey	AS	38.49	38.46	195	409	1.51	6
GLWD00001076	Dukan	Iraq	AS	36.10	44.92	120	95	1.52	6
GLWD00000279	Assad	Syrian Arab Republic	AS	36.08	38.07	637	175	1.64	6
GLWD00000876	Weishan	China	AS	34.60	117.27	175	157	1.51	6
GLWD00001430	Luoma	China	AS	34.11	118.21	248	192	1.53	6
GLWD00000937	Rana Pratap	India	AS	24.83	75.60	171	146	1.82	6
GLWD00000347	Gandhisagar	India	AS	24.44	75.51	524	44	1.84	6
HYLA00001496	None	India	AS	22.80	80.03	153	98	1.78	6
HYLA00001497	Bango	India	AS	22.67	82.63	104	65	1.82	6
GLWD00000249	Hirakud	India	AS	21.66	83.73	501	145	1.86	6
HYLA00001503	None	India	AS	21.47	84.96	311	82	1.77	6
GLWD00000603	Ubol Ratana	Thailand	AS	16.70	102.60	313	39	1.56	6
GLWD00000498	Nagarjuna	India	AS	16.23	79.07	196	1124	1.68	6
GLWD00000289	Srisailam Reservoir	India	AS	16.03	78.08	536	393	1.62	6
GLWD00000528	Tungabhadra	India	AS	15.17	76.23	353	82	1.75	6
HYLA00001530	Pasak Chonlasit	Thailand	AS	14.99	101.05	115	112	1.62	6
GLWD00000330	Sinakharin	Thailand	AS	14.72	99.04	346	32	1.70	6
HYLA00001545	None	Burkina Faso	AF	11.65	-0.76	168	211	1.59	6
GLWD00000475	Tiga	Nigeria	AF	11.39	8.44	108	61	1.72	6
GLWD00000485	Lagos	Nigeria	AF	6.53	3.54	630	76	1.68	6
HYLA00001611	Sulunga	United Republic of Tanzania	AF	-6.09	35.19	802	31	1.63	6
HYLA00001639	None	Australia	OC	-20.20	127.45	127	447	1.58	6
GLWD00000556	Marion	United States	NA	33.53	-80.46	62	604	1.69	6
HYLA00010381	None	Paraguay	SA	-26.17	-57.48	44	40	1.59	6
GLWD00002285	Ebeyty	Russian Federation	EU	54.65	71.74	83	94	1.55	6
GLWD00002239	Uryum	Russian Federation	EU	54.55	78.49	77	148	1.61	6

id	Name	Countries	Continent	lat	lon	Lake area (km2)	Catch area / lake area	95ile SPI	Cluster 20yr
HYLA00013471	None	Russian Federation	EU	53.53	78.56	41	194	1.57	6
GLWD00002057	Ulken-Azhbolat	Kazakhstan	AS	53.28	77.46	92	210	1.56	6
HYLA00013521	None	Russian Federation	EU	53.00	45.33	86	160	1.58	6
HYLA00013575	None	Kazakhstan	AS	52.69	65.84	51	80	1.51	6
GLWD00003421	Koybagar	Kazakhstan	AS	52.61	65.59	62	44	1.56	6
GLWD00003500	Maraldy	Kazakhstan	AS	52.32	77.77	54	33	1.71	6
HYLA00013919	None	Mongolia	AS	48.64	114.41	65	149	1.73	6
HYLA00013927	None	Ukraine	EU	48.59	26.98	75	540	1.57	6
HYLA00013995	None	Ukraine	EU	47.54	33.63	15	30	1.56	6
HYLA00014041	None	China	AS	46.82	125.14	50	37	1.66	6
HYLA00014153	None	China	AS	45.92	124.45	74	404	1.62	6
GLWD00002018	Yueliang	China	AS	45.71	123.87	99	428	1.61	6
HYLA00014305	None	Romania	EU	44.16	27.64	20	134	1.65	6
GLWD00000564	Sudoche-Ko'L	Uzbekistan	AS	43.50	58.40	58	123	1.62	6
HYLA00014360	None	Kazakhstan	AS	43.36	73.97	47	567	1.54	6
HYLA00015361	None	India	AS	29.58	78.78	47	68	1.59	6
GLWD00001501	Matatila-Dam	India	AS	25.05	78.32	66	311	1.96	6
HYLA00015502	Rajghat	India	AS	24.68	78.27	47	360	1.83	6
HYLA00015606	None	India	AS	21.32	78.06	62	68	1.92	6
HYLA00015626	None	Myanmar	AS	20.54	96.92	48	57	1.74	6
HYLA00015638	None	India	AS	19.79	77.32	82	54	1.71	6
HYLA00015714	None	India	AS	16.36	77.65	28	4691	1.66	6
GLWD00003607	Boraphet	Thailand	AS	15.70	100.23	44	82	1.64	6
HYLA00015755	None	Viet Nam	AS	14.31	107.85	45	163	1.63	6
HYLA00015805	None	Nigeria	AF	11.70	8.01	65	59	1.79	6
HYLA00015857	None	Nigeria	AF	8.17	5.60	25	63	1.57	6
HYLA00016311	None	Mozambique	AF	-24.46	33.26	54	69	1.57	6
GLWD00001616	Poelela	Mozambique	AF	-24.54	35.05	88	165	1.62	6
GLWD00007840	Loskop	South Africa	AF	-25.44	29.29	24	522	1.51	6
GLWD00010694	Hartbeespoort	South Africa	AF	-25.75	27.86	17	239	1.52	6
CGL200000007	Nwetwe-Pan	Botswana	AF	-20.64	25.29	2590	232	1.72	6
GLWD00000061	Volgogradskoye	Russian Federation	EU	50.30	45.86	2613	520	1.51	6
GLWD00000087	Kremenshugskoye	Ukraine	EU	49.38	32.38	1849	210	1.73	6
GLWD00000361	Dnieprodzerzhinsk	Ukraine	EU	48.83	34.11	507	868	1.59	6
GLWD00000460	Hendrik Verwoerd	South Africa	AF	-30.63	25.79	294	239	1.57	6
GLWD00000509	Dniester-Estuary	Republic of Moldova;Ukraine	EU	46.23	30.34	370	197	1.58	6
GLWD00001059	Ukal	India	AS	21.35	73.78	370	168	1.83	6
GLWD00000287	Gaoyou	China	AS	32.78	119.22	703	244	1.64	6
GLWD00001206	Dushan	China	AS	34.98	116.85	238	100	1.52	6

id	Name	Countries	Continent	lat	lon	Lake area (km2)	Catch area / lake area	95ile SPI	Cluster 20yr
HYLA00001257	Huoshaohei-Talahong	China	AS	46.75	124.19	430	64	1.63	6
GLWD00000471	Kanivs'Ke	Ukraine	EU	50.12	30.90	470	729	1.57	6
GLWD00000217	Grande	Brazil	SA	-20.26	-48.87	349	339	1.56	6
HYLA00005962	None	Canada	NA	55.78	-105.14	62	36	1.65	6
HYLA00013715	None	Kazakhstan	AS	50.90	74.01	59	76	1.58	6
HYLA00015220	None	Egypt	AF	31.29	32.15	78	148	1.94	6